

Eastern Pacific Warm Pool paleosalinity and climate variability: 0-30 ky

H. M. Benway¹, A.C. Mix¹, B. A. Haley², G. P. Klinkhammer¹

*1. College of Oceanic and Atmospheric Sciences, Oregon State University, Corvallis,
Oregon 97331 USA*

*2. Leibniz-Institute of Marine Sciences, IFM-GEOMAR, East Shore Campus, Kiel,
GERMANY*

Abstract

Multi-proxy geologic records of $\delta^{18}\text{O}$ and Mg/Ca in fossil foraminifera from sediments under the Eastern Pacific Warm Pool (EPWP) region west of Central America document variations in upper ocean temperature, pycnocline strength, and salinity (*i.e.*, net precipitation) over the past 30 ky. Although evident in the paleotemperature record, there is no glacial-interglacial difference in paleosalinity, suggesting that tropical hydrologic changes do not respond passively to high-latitude ice sheets and oceans. Millennial variations in paleosalinity with amplitudes as high as ~ 4 PSU occur with a dominant period of ~ 3 -5 ky during the glacial/deglacial interval and ~ 1.0 -1.5 ky during the Holocene. The amplitude of the EPWP paleosalinity changes greatly exceeds that of published Caribbean and western tropical Pacific paleosalinity records. EPWP paleosalinity changes correspond to millennial-scale climate changes in the surface and deep Atlantic and the high northern latitudes, with generally higher (lower) paleosalinity during cold (warm) events. In addition to Intertropical Convergence Zone (ITCZ) dynamics, which play an important role in tropical hydrologic variability, changes in Atlantic-Pacific moisture transport, which is closely linked to ITCZ dynamics, may also contribute to hydrologic variations in the EPWP. Calculations of interbasin salinity average and interbasin salinity contrast between the EPWP and the Caribbean help differentiate long-term changes in mean ITCZ position and Atlantic-Pacific moisture transport, respectively.

1. Introduction

High net precipitation ($P-E > 0$) maintains relatively low sea-surface salinities and a strong, shallow pycnocline in the eastern Pacific warm pool (EPWP) region west of Central America. In contrast, the Caribbean has high salinity due to high net evaporation ($P-E < 0$) (Fig. 1). Net export of freshwater in the form of water vapor from the Atlantic basin helps to maintain the salinity contrast between the Atlantic and Pacific Oceans, an important control of global thermohaline circulation, oceanic heat transport, and climate [Zaucker *et al.*, 1994; Rahmstorf, 1995]. A significant portion of this Atlantic freshwater export occurs across the Panama Isthmus [Oort, 1983; Weyl, 1968]. Here, low-level (>850 mb) northeasterly winds transport water vapor from Atlantic and Caribbean sources into the EPWP region, where high sea-surface temperatures (SSTs) sustain atmospheric convection, resulting in heavy rainfall on the Pacific side of the Isthmus [Magaña *et al.*, 1999]. Estimates of this net freshwater transport based on modern atmospheric general circulation model (AGCM) simulations and climatologic data range from 0.13 Sv [Zaucker and Broecker, 1992] to 0.45 Sv [Baumgartner and Reichel, 1975; Manabe and Stouffer, 1988] ($1 \text{ Sv} = 10^6 \text{ m}^3 \text{ s}^{-1}$).

The low salinity EPWP (Fig. 1) corresponds generally to the region of high net precipitation near the Panama Isthmus, and extends westward under the ITCZ at 8-10° N. However, on an annual average, two separate regions of highest net precipitation are observed (near Costa Rica at roughly 5-9° N, 82-87° W, and near Colombia at roughly 4-7° N, 75-79° W). Satellite wind and altimetry observations in the EPWP region document seasonal variations in winds that accompany the meridional migration of the intertropical convergence zone (ITCZ) [Rodríguez-Rubio *et al.*, 2003]. During boreal summer when

the ITCZ is in its northernmost position, the southeasterly trades strengthen and curl to the northeast upon crossing the Equator (due to the change in sign of the Coriolis parameter), delivering more Pacific moisture to the EPWP region. The westerly Chocó Jet, which is more prevalent during this season, delivers atmospheric moisture to coastal Colombia [*Poveda and Mesa, 2000; Martínez et al., 2003*], yielding a pronounced maximum in precipitation between 4-7° N. Reduced convection accompanied by a brief intensification of the northeasterly trades occurs during the midsummer drought in July and August [*Magaña et al., 1999*]. In October, when the ITCZ starts to migrate southward, the northeasterly trades strengthen, contributing more Caribbean and tropical Atlantic moisture [*Xu et al., 2005*], yielding another maximum in precipitation rate near Costa Rica. The duration of the Central American rainy season depends in part on the relationship between tropical Atlantic and eastern Pacific SST patterns about the ITCZ [*Enfield and Alfaro, 1999*].

In addition to the large-scale flow of moist air across the Panama Isthmus, the relatively strong northeasterly trades accelerate through topographic gaps in the Central American cordillera, resulting in smaller-scale features such as the northeasterly Papagayo Jet [*Xie et al., 2005*] and the northerly Panama Jet [*Chelton et al., 2000*]. Although these jets are typically associated with localized wind-driven upwelling and transient SST anomalies, they do not strongly affect the total amount of Atlantic moisture transported across the Panama Isthmus [*Xu et al., 2005*]. These local SST anomalies combined with increased subsidence on the Pacific coast of Central America during

winter months when the northeasterly trades are stronger, displace the ITCZ to the southern edge of the EPWP [Xu *et al.*, 2005].

Seawater and rainwater $\delta^{18}\text{O}$ measurements from the EPWP region [Benway and Mix, 2004] indicate that in addition to local Pacific moisture, Atlantic and Caribbean moisture sources comprise a significant portion of the stable isotope budget in this region.

Precipitation from local Pacific sources is less depleted in ^{18}O (average = -5 ‰) [Benway and Mix, 2004], whereas water vapor that is transported across Central America from distant sources in the Atlantic and Caribbean is more depleted in ^{18}O because of long distance transport and orographic distillation. Costa Rican surface water $\delta^{18}\text{O}$ decreases by 6 to 8 ‰ upon crossing the Central American Cordillera, and values remain low along the Pacific coast relative to the Caribbean coast [Lachniet and Patterson, 2002].

In addition to high latitude freshwater forcing, a number of modeling studies demonstrate that the global thermohaline circulation is also sensitive to tropical freshwater forcing [Latif *et al.*, 2000; Latif, 2001; Vellinga and Wu, 2004; Goelzer *et al.*, submitted]. Although the role of vapor transport in maintaining the modern inter-ocean salinity contrast is known [Zaucker *et al.*, 1994], variations through time are unconstrained. Variations of terrigenous sediments in Cariaco Basin have been linked to high interstadial rainfall in northern South America and a higher net export of moisture from the Atlantic to the Pacific during northward excursions of the ITCZ [Peterson *et al.*, 2000]. Numerical models suggest that vapor transport increases during warm phases of the El Niño-Southern Oscillation (ENSO) [Schmittner *et al.*, 2000], and that long-term ENSO variability may modify ocean salt balance and North Atlantic Deep Water

formation [Schmittner and Clement, 2002]. AGCM simulations suggest that vapor transport increased during glacial times due to stronger easterly winds, although this effect may be partly compensated by lower atmospheric moisture associated with cool climates [Hostetler and Mix, 1999]. Since Atlantic and Caribbean moisture sources comprise a significant portion of the EPWP precipitation budget [Benway and Mix, 2004], sea-surface paleosalinity changes should in part reflect changes in the hydrologic balance (P-E) associated with cross-isthmus vapor transport.

2. Materials and Methods

Chemical measurements of foraminiferal shells preserved in marine sediments help to constrain changes in sea-surface salinity, and by inference, net precipitation in the EPWP and its relationship to global climate and deep ocean circulation. Sediment cores ME0005A-43JC (7° 51.35'N, 83° 36.50'W, 1368 m) and Ocean Drilling Program (ODP) Site 1242 (7° 51.35'N, 83° 36.42'W, 1364 m) (Fig. 1) provide well-preserved replicate records sampled at ~200 year intervals over the past 30,000 years. Radiocarbon chronologies are expressed as calendar ages between 0 and 20 ka [Stuiver and Reimer, 1993], and correlation of stable isotope records to other well-dated records extends age control to 30 ka [Shackleton et al., 2000]. Sedimentation rates are 10-12 cm ky⁻¹, sufficient to resolve millennial-scale events in detail.

The oxygen isotope composition of foraminiferal calcite ($\delta^{18}\text{O}_c$) reflects both temperature and ambient seawater composition ($\delta^{18}\text{O}_{\text{sw}}$). Independent estimates of calcification temperature from Mg/Ca measurements of *Globigerinoides ruber*, based on

flow-through leaching [Haley and Klinkhammer, 2002; Benway et al., 2003] deconvolve the temperature and water mass effects on $\delta^{18}\text{O}_c$. Modern regional $\delta^{18}\text{O}_{sw}$ -S relationships [Benway and Mix, 2004] provide a basis for estimating paleosalinity. Over the past ~30 ky, sealevel reconstructions provide reasonable corrections for the global changes in $\delta^{18}\text{O}_{sw}$ driven by changing ice volume [Clark and Mix, 2002; Waelbroeck et al., 2002].

2.1. Stable Isotopes

Isotope measurements were made at 2-3 cm intervals in ME0005A-43JC and 4-cm intervals in ODP 1242. Sediment samples were cleaned and sieved with deionized water and calgon, and coarse fractions were dried at 40°C. Specimens of *G. ruber* (*N. dutertrei*) were picked from the 250-355 μm (355-425 μm) size fraction. Fifteen (ten) specimens of *G. ruber* (*N. dutertrei*) were used for each stable isotope measurement. In preparation for stable isotope analysis, samples were sonicated in deionized water and 95% ethanol. Samples were dried at 40°C for 12-24 hours, and analyzed at Oregon State University on a Finnigan-MAT 252 stable isotope ratio mass spectrometer equipped with a Kiel-III carbonate device. Samples were reacted at 70°C in phosphoric acid, and all data are reported relative to the Pee Dee Belemnite (PDB) standard via our internal standard, which is regularly calibrated against NBS-19 and NBS-20.

2.2. Mg/Ca

Mg/Ca ratios were measured on *G. ruber* (~10-20 specimens) collected from the same samples as those measured for stable isotopes using a flow-through technique

[*Haley and Klinkhammer, 2002; Benway et al., 2003*] that combines ion chromatography and inductively coupled plasma mass spectrometry (ICP-MS) in a series of cleaning and dissolution reactions monitored continuously with time-resolved analysis (TRA). This method minimizes analytical biases associated with sample cleaning, minor diagenetic influences, and partial dissolution at the sea floor [*Klinkhammer et al., 2004*].

Flow-through analysis includes measurement of a cocktail of internal standards (covering the mass range of interest) to monitor and correct for minor instrument drift, as well as a suite of external reagent standards (Ca, Mg, Sr, Al, Mn) that calibrate instrument response over a reasonable concentration range for biogenic calcite (which is linear). In addition, two external standards, NIST-1c argillaceous limestone and a homogeneous marble called the “Wiley standard,” which are leached in the same way as foraminifera samples, serve as additional monitors of intra- and inter-run consistency. Finally, standardization of daily runs is carefully checked by analysis of overlapping sections of core and replication on different days, with minor adjustments (within the errors of daily calibration) to minimize daily offsets.

Samples from ME0005A-43JC were cracked and sonicated in deionized water and 95% ethanol to remove clays. The homogenized samples were then split between stable isotope and Mg/Ca analysis. Samples from ODP Site 1242 were analyzed according to recent developments in the flow-through technique [*Klinkhammer et al., 2004*]. A correction was applied to older Mg/Ca data to account for a systematic offset of 0.3 mmol/mol that reflects recent improvements in standardization.

2.3. Calculations of seawater $\delta^{18}\text{O}$ – temperature and sealevel corrections

Calcification temperature was calculated from Mg/Ca using $\text{SST} = \ln(\text{Mg/Ca}/0.38)/0.09$ [Anand *et al.*, 2003]. No corrections are needed for preservation effects, because of the shallow water depth of the sites and because the flow-through Mg/Ca analyses are relatively insensitive to such effects [Benway *et al.*, 2003; Klinkhammer *et al.*, 2004]. We used these temperature estimates, in combination with stable isotope analyses, calculated $\delta^{18}\text{O}_{\text{sw}}$, based on the empirical isotopic paleotemperature equation developed for *G. ruber* [Thunell *et al.*, 1999], which is the same as a “high-light” equation developed for *Orbulina universa* [Bemis *et al.*, 1998].

We applied an ice volume correction based on coral [Clark and Mix, 2002] (0-21 ka) and benthic foraminiferal isotope [Waelbroeck *et al.*, 2002] (21-30 ka) sealevel reconstructions to our $\delta^{18}\text{O}_{\text{sw}}$ records using Gaussian interpolation. To demonstrate the potential uncertainty associated with the ice volume calculation, we show a range of corrected $\delta^{18}\text{O}_{\text{sw}}$ (Fig. 3d) estimates based on a $\delta^{18}\text{O}_{\text{sw}}$ -sealevel scaling range of 0.0075-0.0100 ‰ m^{-1} decrease in relative sea level (RSL).

2.4. Age Model

Age models for ME0005A-43JC and ODP 1242 are based on a combination of $\delta^{18}\text{O}$ stratigraphy [Shackleton *et al.*, 2000] and six accelerator mass spectrometry (AMS) ^{14}C dates (*N. dutertrei*) from ME0005A-43JC. The Calib (version 5.0.1) program [Stuiver and Reimer, 1993] was used to convert ^{14}C ages to calendar ages, assuming a reservoir

age of 558 years, the regional average for the west coast of Central America [Stuiver and Reimer, 1993]. To apply the radiocarbon dates from 43JC to Site 1242, 1242 data were first expressed on 43JC pseudo-depths, based on depth-domain correlation of variations in stable isotope, Mg/Ca, and sediment density data.

2.5. Error Analysis

Analytical precision of $\delta^{18}\text{O}_c$ measurements is ± 0.06 ‰, and that of flow-through Mg/Ca measurements is ± 0.10 mmol/mol, which translates to $\pm 0.3^\circ\text{C}$ for the temperature range considered here. In addition, the error associated with the Mg/Ca-temperature calibration equation [Anand *et al.*, 2003] is $\pm 0.5^\circ\text{C}$. The compounded (analytical + calibration) temperature error is $\pm 0.6^\circ\text{C}$. The slope error in the paleotemperature equation [Bemis *et al.*, 1998; Thunell *et al.*, 1999] used to calculate $\delta^{18}\text{O}_{sw}$ yields an additional error of ± 0.07 ‰. Assuming a 1σ normal distribution in the Mg/Ca and $\delta^{18}\text{O}_c$ measurements, the compounded $\delta^{18}\text{O}_{sw}$ error is ± 0.3 ‰, translating to a paleosalinity error of ± 1.2 PSU, based on application of the modern $\delta^{18}\text{O}_w$ -S relationship. Standard error of paleosalinity estimates based on the modern $\delta^{18}\text{O}_w$ -S relationship for the EPWP region is ± 0.2 PSU [Benway and Mix, 2004] for a total salinity error of ± 1.4 PSU. Deviations in the $\delta^{18}\text{O}_{sw}$ -S relationship through time may generate paleosalinity errors ranging from 0.1-2.0 PSU with the largest errors attributed to changes in mean $\delta^{18}\text{O}_{precipitation}$ [Benway and Mix, 2004].

3. Results and Discussion

3.1. Modern Sediments

Regional core-top $\delta^{18}\text{O}_c$ and Mg/Ca measurements confirm near-surface calcification for *G. ruber* and suggest that the equation that relates temperature to Mg/Ca, as calibrated in well-preserved samples in the Atlantic [Anand *et al.*, 2003] is a good approximation for geologic samples measured in the Pacific using our flow-through method (Fig. 2).

The $\delta^{18}\text{O}_c$ contrast between two species of planktonic foraminifera, *G. ruber* and *Neogloboquadrina dutertrei*, which lives in the thermocline [Spero *et al.*, 2003] (Fig. 2) provides an estimate of upper ocean density gradients. The primary control of $\delta^{18}\text{O}_c$ in regional surface waters from the EPWP is salinity (driven largely by net precipitation with relatively minor contributions from river runoff) [Benway and Mix, 2004], whereas in subsurface waters it is temperature (related to upwelling; Fig. 1, inset).

3.2. The Past 30,000 Years

Over the past 30 ky, sharp decreases in *G. ruber* $\delta^{18}\text{O}_c$ at 11.2 ka and 16.3 ka reflect the deglacial transition (Fig. 3a). The isotopic contrast between *G. ruber* and *N. dutertrei* (Fig. 3b) reveals significant differences between glacial (15-25 ka, 2.3 ± 0.3 ‰) and Holocene (0-10 ka, 2.8 ± 0.3 ‰) times, with low but variable contrast during the deglacial transition (10-15 ka, 2.4 ± 0.3 ‰). Mg/Ca in *G. ruber* (Fig. 3c) documents a glacial (19-23 ka) to late Holocene (3-5 ka) temperature change of $2.8^\circ \pm 0.8^\circ\text{C}$. Abrupt warming of $\sim 1\text{-}2^\circ\text{C}$, which started at ~ 19 ka, would reduce *G. ruber* $\delta^{18}\text{O}_c$ by ~ 0.6 ‰,

suggesting that much of the glacial-interglacial change in the isotopic difference between *G. ruber* and *N. dutertrei* may reflect changes in sea-surface temperatures.

The apparent difference in timing of changes in Mg/Ca temperature and $\Delta\delta^{18}\text{O}_{\text{dut-ruber}}$, however, indicates that changes in subsurface watermasses were decoupled from changes in sea-surface temperature; for example, an increase in $\delta^{18}\text{O}$ of *N. dutertrei* and relatively high $\Delta\delta^{18}\text{O}_{\text{dut-ruber}}$ from 13-14 ka coincides with the Antarctic Cold Reversal [Jouzel *et al.*, 1995], consistent with transmission of southern ocean climate changes in subsurface water masses.

Removal of local Mg/Ca temperature and global ice volume [Clark and Mix, 2002; Waelbroeck *et al.*, 2002] effects on *G. ruber* $\delta^{18}\text{O}_c$ yields an estimate of upper ocean $\delta^{18}\text{O}_{\text{sw}}$ (Fig. 3d, 4c) that shows a dominant period of ~3-5 ky during glacial/deglacial time (~10-25 ka), and variations with a period of ~1.0-1.5 ky during the Holocene (0-10 ka) (Fig. 5). Uncertainties in ice-volume corrections have negligible effects on the timing or amplitude of the observed millennial-scale $\delta^{18}\text{O}_{\text{sw}}$ changes (Fig. 3d).

Measurements of rainwater $\delta^{18}\text{O}$ and the seawater $\delta^{18}\text{O}$ -salinity relationship in the EPWP region ($\delta^{18}\text{O}_{\text{sw}} = 0.25S - 8.52$) collectively suggest that the moisture budget for this region is dominated by precipitation, about half of which reflects long-distance transport [Benway and Mix, 2004]. Assuming that the modern EPWP $\delta^{18}\text{O}$ -salinity is applicable through time, we calculate large (up to ~4 PSU) millennial-scale sea-surface paleosalinity changes (Fig. 4c) in the EPWP. The amplitude of EPWP paleosalinity changes for this interval exceeds that of the Caribbean [Schmidt *et al.*, 2004] (Fig. 4c) and the western Pacific [Stott *et al.*, 2002].

Despite an appreciable glacial-interglacial SST difference, there is no significant contrast between paleosalinities averaged over the glacial (~15-25 ka, 34.8 ± 1.2 PSU) and Holocene (~0-10 ka, 34.5 ± 1.1 PSU) intervals, suggesting that there is little or no direct effect of glacial boundary conditions on surface ocean salinities in the EPWP. Though more highly variable during the glacial interval, Caribbean records [*Schmidt et al.*, 2004] also do not show a significant glacial-interglacial salinity contrast. These results are in apparent conflict with recent modeling [*Chiang et al.*, 2003] and paleoclimatic [*Peterson et al.*, 2000; *Koutavas et al.*, 2002] evidence for a southward migration of the ITCZ in response to LGM boundary conditions, but are consistent with the model results of Takahashi and Battisti (2005) that suggest stabilization of the Pacific ITCZ in the northern hemisphere due to Andean orography. A shift in ITCZ position in both the Atlantic and Pacific would likely yield a glacial-interglacial salinity difference in both of these regions, with higher glacial salinities (relative to late Holocene) at both sites, since they are in the same latitudinal band. A southward shift in the Atlantic alone would imply a salinity increase in the Caribbean, and greater interbasin salinity contrast.

3.2. Comparison to Existing Paleoclimate Records

Relatively low EPWP paleosalinity is associated with millennial-scale climate events documented elsewhere, including intervals of sea-level rise (the 19 ka early rise and Terminations 1a and 1b [*Clark and Mix*, 2002]), warmth in the tropical [*Lea et al.*, 2003] and subtropical [*Bard*, 2002] Atlantic and in Greenland (the early Holocene, the Bølling/Allerød interval, and a weak event near 19 ka) [*Grootes and Stuiver*, 1997],

increased terrigenous flux (increased rainfall) in the Cariaco Basin [*Peterson et al.*, 2000; *Haug et al.*, 2001], and higher rates of Atlantic meridional overturning circulation (MOC) indicated by $^{231}\text{Pa}/^{230}\text{Th}$ [*McManus et al.*, 2004]. North Atlantic benthic $\delta^{13}\text{C}$ records from MD95-2042 (37° 48'N, 10° 10'W, 3146 m) [*Shackleton et al.*, 2000], V30-51K (19° 52'N, 19° 55'W, 3409 m) [*Mix*, 1985], and ODP Site 980 (55° 29'N, 14° 42'W, 2179 m) [*McManus et al.*, 1999; *Oppo et al.*, 2003] corroborate deep ocean circulation changes over the past 20 ky (Fig. 4) with higher (lower) benthic $\delta^{13}\text{C}$ corresponding to increased (decreased) MOC. Higher EPWP paleosalinity is generally associated with cooling in the tropical and subtropical Atlantic and Greenland, reduced rainfall in the Cariaco Basin, and reduced Atlantic thermohaline overturn, including Heinrich Events 2 and 3 (H2, H3), the Younger Dryas period, and a possible Holocene event near 8-8.5 ka. EPWP paleosalinity is highly variable during the LGM with generally higher paleosalinity from ~23-21 ka, followed by a marked decline that occurs ~21-19 ka. This LGM pattern contrasts with the record from the Caribbean [*Schmidt et al.*, 2004], where paleosalinity starts lower (~23-21 ka) and rises during the ~21-19 ka interval.

3.3. Mechanisms of Climate Variability

Numerous modeling studies [*Vellinga and Wood*, 2002; *Zhang and Delworth*, 2005; *Dahl et al.*, 2005] show a southward migration of the ITCZ, especially in the Atlantic sector, in response to reduced Atlantic thermohaline overturn. While some North Atlantic freshwater hosing experiments yield hydrologic impacts that expand into the tropical Pacific [*Vellinga and Wood*, 2002 (North Atlantic freshwater forcing = 16 Sv for 1 year);

Zhang and Delworth, 2005 (North Atlantic freshwater input = 0.6 Sv for 60 years)], other simulations [*Dahl et al., 2005* (North Atlantic freshwater input = 0.1 Sv for 100 years)] only show a strong response in the tropical Atlantic. The modeled response of the ITCZ to reduced Atlantic meridional overturning circulation (MOC) could in part explain our observation of higher EPWP paleosalinity during cold events with reduced MOC (Fig. 4).

Because the Pacific and Caribbean sites are in the same latitudinal band, changes in mean ITCZ position and/or intensity should yield a roughly similar paleosalinity response at both sites. On the other hand, divergence of Caribbean and EPWP paleosalinities may reflect net moisture export to the Pacific. Cross-spectra comparing EPWP and Caribbean $\delta^{18}\text{O}_{\text{sw}}$ [*Schmidt et al., 2004*] records show limited coherence in the millennial frequency band, and phase calculations suggest that paleosalinity changes at the Caribbean site lead those at the EPWP site (Fig. 6). This phasing implicates other processes in addition to ITCZ dynamics to explain the variability observed in these tropical records.

It is difficult to characterize large-scale processes like ITCZ dynamics and cross-isthmus vapor transport with paleosalinity records from only two sites. Ideally, these processes would be described with a network of tropical and subtropical sites from the Caribbean, Atlantic and Pacific. However, in a preliminary attempt to examine these processes in our records, we calculated variations in interbasin (Caribbean vs. EPWP) paleosalinity average (Fig. 4d) and interbasin paleosalinity difference (Fig. 4e). Both properties were calculated by placing the higher resolution Pacific record on the Caribbean time scale using Gaussian interpolation (time step = 0.1 ky, filter width = 0.4

ky). EPWP and Caribbean paleosalinities from both sites were calculated using modern regional $\delta^{18}\text{O}_{\text{sw}}$ -S relationships [Benway and Mix, 2004; Schmidt et al., 2004].

The potential chronological error associated with comparing the two time series is calculated by using 2-sigma error bars on radiocarbon dates to construct the oldest and youngest possible age models for both records. The gray curves in Figs. 4d and 4e encompass the largest possible chronological error ranges in the difference and average calculations. Although the amplitudes are affected in parts of each record, the timing and patterns of variability are generally the same, suggesting that these comparisons of EPWP and Caribbean records are robust to existing chronologic uncertainties.

Relatively low interbasin average salinity, which should represent a more northern position of the ITCZ, occurs ~21-19 ka, marking the end of the LGM, and during the Bølling/Allerød and early Holocene climatic optimum warm periods (Fig. 4d). During colder intervals such as the Younger Dryas, H1, H2, and H3, the interbasin average is relatively high, perhaps suggesting a more southward position of the ITCZ. Apart from the LGM interval, sediment reflectance records from Cariaco Basin [Peterson et al., 2000] are consistent with this pattern (Fig. 4b), with wetter (drier) conditions during warm (cold) intervals of the last 30 ky. However, the glacial-interglacial difference that has been observed in the Cariaco Basin records [Peterson et al., 2000; Haug et al., 2001] is not reflected in the interbasin average salinity.

The average salinity difference between the EPWP and Caribbean (Fig. 4e) is 1.2 PSU, and as with the interbasin average, there is no significant difference between average glacial and average Holocene conditions, suggesting that glacial boundary

conditions alone do not control westward vapor transport. A maximum contrast of ~2-3 PSU occurs toward the end of the LGM (~21-19 ka). The divergence of the Pacific and Caribbean paleosalinities at this time may reflect relatively high vapor transport at a time when the ITCZ is relatively far to the north, as reflected by relatively low interbasin average salinity. Following the LGM, higher than average interbasin contrast occurs in general during warmer intervals such as the Bølling/Allerød and early Holocene climatic optimum, and lower than average interbasin contrast corresponds to colder periods such as the Younger Dryas and H1 (Fig. 4e), although the timing of abrupt changes is not identical to the high-latitude events. The approximate anti-phasing of the interbasin salinity contrast and interbasin salinity average records throughout the past 30 ky (Fig. 4) suggests increased (decreased) vapor transport during periods of relatively low (high) background salinity, indicative of a northward (southward) ITCZ position, as described by *Peterson et al.* [2000]. This connection, if correct, would suggest that the modern seasonal cycle, which is characterized by stronger northeasterly trades and increased cross-isthmus transport (as evidenced by minimum sea surface salinities during winter months at this EPWP site) during southward excursions of the ITCZ, is not an analog for longer-term variations in the past.

Cross-spectra comparing both EPWP $\delta^{18}\text{O}_{\text{sw}}$ and interbasin contrast with Atlantic MOC strength [*McManus et al.*, 2004] reveal coherence at periods of 3-5 ky (Fig. 7), the dominant period observed in the glacial/deglacial portion of the Pacific $\delta^{18}\text{O}_{\text{sw}}$ record (Fig. 5). Given the chronological uncertainties in the interbasin contrast record, cross-spectra were calculated across the full range of potential interbasin contrast chronologies

(gray lines, Fig. 4e) propagated from 2-sigma ^{14}C age ranges in the Pacific and Caribbean $\delta^{18}\text{O}_{\text{sw}}$ records (i.e., youngest plausible Pacific chronology versus oldest plausible Caribbean chronology, and vice versa). The coherence between interbasin contrast and Atlantic MOC at periods of 3-5 ky is robust to these age model uncertainties. Phase calculations suggest the possibility of a lead of interbasin contrast over Atlantic MOC by as much as ~ 1 ky, but large error bars on the phases preclude accurate estimates of leads and lags within the limits of chronological uncertainty. The EPWP $\delta^{18}\text{O}_{\text{sw}}$ and interbasin contrast records are also coherent with Atlantic $\delta^{13}\text{C}$ records [McManus *et al.*, 1999; Oppo *et al.*, 2003; McManus *et al.*, 2004] at periods of 3-5 ky. The lack of glacial-interglacial contrast in the hydrologic system, and the possibility that tropical changes may lead high-latitude climate and circulation changes, open the possibility that North Atlantic circulation is in part influenced by changes in westward vapor transport, via control of the North Atlantic salinity budget and thermohaline overturn, as originally suggested by Weyl [1968]. The sensitivity of this coupled system may depend on climate stability and the mean state of the North Atlantic [Schmittner and Clement, 2002].

One plausible tropical mechanism for changing inter-ocean vapor transport calls on the relative roles of atmospheric moisture content and tropospheric wind speed [Hostetler and Mix, 1999]. Cooling of the tropical and subtropical oceans would reduce moisture content of the lower atmosphere. Reduced evaporation and export of freshwater to the Pacific would over time decrease Atlantic salinity, thereby reducing North Atlantic Deep Water (NADW) formation [Zaucker *et al.*, 1994; Rahmstorf, 1995]. At the same time, a diminished supply of Atlantic moisture to the EPWP region would result in less rainfall

and higher Pacific salinities, with potential to support more rapid ventilation of intermediate and/or deep waters of the North Pacific [Zheng *et al.*, 2000].

Tropical cooling (relative to mid-to-high latitudes) would also reduce trade wind intensities and cyclogenesis, which both play a role in westward vapor transport [Benway and Mix, 2004], and such effects offer the potential to amplify effects of atmospheric moisture at millennial scales. Lack of significant glacial-interglacial change of inter-basin salinity contrast, however, may suggest that at longer time scales the competing effects of lower atmospheric vapor and higher wind speeds (associated with compressed thermal gradients to high latitudes at the LGM), were approximately balanced.

Following reduction of Atlantic meridional overturning circulation, buildup of oceanic heat in the tropical and subtropical Atlantic would increase atmospheric moisture and net westward vapor transport, eventually leading to increased Atlantic salinities and a return to the "NADW-on" mode. This set of connections based on varying cross-isthmus vapor transport could conceivably form an Atlantic-Pacific Salt Oscillator, analogous to a salt oscillator previously envisioned within the North Atlantic [Broecker *et al.*, 1990].

4. Conclusions

Late Pleistocene reconstructions document large (~2-4 PSU) paleosalinity variations in the EPWP region that correspond with well-documented climate events in other tropical and high latitude proxy records, suggesting that tropical hydrologic changes play an important role in global climate. EPWP paleosalinity records likely reflect both

changes in the total rate of westward vapor transport, and changes in moisture sources related to shifts in the position of the ITCZ.

Comparisons of EPWP paleosalinity records with Caribbean records from the same latitudinal band show much higher amplitude variability in the EPWP, and limited coherence in the millennial frequency band. Using calculations of salinity average and salinity difference between the EPWP and Caribbean records, we attempt to differentiate changes in mean ITCZ position (which should yield salinity changes of the same sign), and Atlantic-Pacific vapor transport (which should yield salinity changes of the opposite sign), respectively.

Approximate anti-phasing of the interbasin average and interbasin contrast in paleosalinity suggests that strongest westward vapor transport occurs when the ITCZ is in a northerly position. This pattern of change is opposite the sense of the modern seasonal cycle, suggesting that the seasonal cycle may not be a useful analog for longer-term variability in the EPWP.

Comparisons of EPWP paleosalinity and interbasin contrast to Atlantic MOC records suggest a linkage between the tropical hydrologic cycle and global climate and deep ocean circulation changes. One interpretation is that changes in mean ITCZ position respond to changes in high latitude temperature or deep ocean circulation, as observed in several modeling studies. Lack of a significant glacial-interglacial difference in the paleosalinities in this region, however, argues against this option, or requires other compensating changes associated with glacial boundary conditions.

Alternatively, an Atlantic-Pacific salt oscillator, in which tropical climate processes trigger changes in Atlantic-Pacific moisture transport, which in turn alters the salt balance between the Atlantic and Pacific basins, may initiate changes in deep ocean circulation and climate, providing a mechanism in which the tropics serve as a coupled feedback mechanism, rather than a passive response to high-latitude climates. A growing network of high-resolution paleosalinity records from the eastern tropical Pacific and Caribbean will reveal more complete spatial patterns of past tropical hydrologic changes and allow for more robust comparisons between the Pacific and Caribbean, and to records of Atlantic MOC and high latitude temperature.

References

- Anand, P., H. Elderfield, and M. H. Conte (2003), Calibration of Mg/Ca thermometry in planktonic foraminifera from a sediment trap time series, *Paleoceanography* 18, doi:10.1029/2002PA000846.
- Bard, E. (2002), Abrupt climate change over millennial time scales: climate shock, *Physics Today* 55, 32-38.
- Baumgartner, A., and E. Reichel (1975), *The World Water Balance*, Elsevier, Amsterdam.
- Bemis, B. E., H. J. Spero, J. Bjima, and D. W. Lea (1998), Reevaluation of the oxygen isotopic composition of planktonic foraminifera: Experimental results and revised paleotemperature equations, *Paleoceanography* 13, 150-160.
- Benway, H. M., A. C. Mix, B. A. Haley, and G. P. Klinkhammer (2003), Adaptation of a flow-through leaching procedure for Mg/Ca paleothermometry: Overcoming the dissolution problem, *Geochem. Geophys. Geosyst.* 4(2) doi: 10.1029/2002GC000312.
- Benway, H. M., and A. C. Mix (2004), Oxygen isotopes, upper-ocean salinity, and precipitation sources in the eastern tropical Pacific, *Earth Planet. Sci. Let.* 224, 493-507.

- Broecker, W., G. Bond, M. Klas, G. Bonani, and W. Wölfli (1990), A salt oscillator in the Glacial Atlantic? *Paleoceanography* 5, 469-477.
- Chelton, D. B., M. H. Freilich, and S. K. Esbensen (2000), Satellite observations of the wind jets off the Pacific coast of Central America. Part II: Relationships and dynamical considerations, *Monthly Weather Review* 128, 2019-2043.
- Chiang, J. C. H., M. Biasutti, and D. S. Battisti (2003), Sensitivity of the Atlantic Intertropical Convergence Zone to Last Glacial Maximum boundary conditions, *Paleoceanography* 18, doi:10.1029/2003PA000916.
- Clark, P. U., and A. C. Mix (2002), Ice sheets and sea level of the Last Glacial Maximum, *Quaternary Science Reviews* 21, 1-7.
- Dahl, K. A., A. J. Broccoli, and R. J. Stouffer (2005), Assessing the role of North Atlantic freshwater forcing in millennial scale climate variability: a tropical Atlantic perspective, *Climate Dynamics* 24, 325-346.
- Enfield, D. B., and E. J. Alfaro (1999), The dependence of Caribbean rainfall on the interaction of the tropical Atlantic and Pacific Oceans, *Journal of Climate* 12, 2093-2103.
- Goelzer, H., A. Levermann, J. Mignot, and S. Rahmstorf (Submitted), Tropical versus high latitude freshwater influence on the Atlantic circulation, *Climate Dynamics*.
- Grootes, P. M., and M. Stuiver (1997), Oxygen 18/16 variability in Greenland snow and ice with 10^3 to 10^5 -year time resolution, *Journal of Geophysical Research* 102, 26,455-26,470.
- Haley, B. A., and G. P. Klinkhammer (2002), Development of a flow-through system for cleaning and dissolving foraminiferal tests, *Chemical Geology* 185, 51-69.
- Haug, G. H., K. A. Hughen, D. M. Sigman, L. C. Peterson, and U. Röhl (2001), Southward migration of the Intertropical Convergence Zone through the Holocene, *Science* 293, 1304-1308.
- Hostetler, S. W., and A. C. Mix (1999), Reassessment of ice-age cooling of the tropical ocean and atmosphere, *Nature* 399, 673-676.
- Joussaume, S., R. Sadourny, and C. Vignal (1986), Origin of precipitating water in a numerical simulation of the July climate, *Ocean-Air Interactions I*, 43-56.
- Jouzel, J., R. Vaikmae, J. R. Petit, M. Martin, Y. Duclos, M. Stievenard, C. Lorius, M. Toots, M. A. Mélières, L. H. Burckle, N. I. Barkov, and V. M. Kotlyakov (1995), The

- two-step shape and timing of the last deglaciation in Antarctica, *Climate Dynamics* 11(3), 151-161.
- Klinkhammer, G. P., B. A. Haley, A. C. Mix, H. M. Benway, and M. Cheseby (2004), Evaluation of automated flow-through time-resolved analysis of foraminifera for Mg/Ca paleothermometry, *Paleoceanography* 19, doi:10.1029/2004PA001050.
- Koutavas, A., J. Lynch-Stieglitz, T. M. Marchitto Jr., and J. P. Sachs (2002), El Niño-like pattern in ice age tropical Pacific sea surface temperature, *Science* 297, 226-230.
- Lachniet, M. S., and W. P. Patterson (2002), Stable isotope values of Costa Rican surface waters, *Journal of Hydrology* 260, 135-150.
- Latif, M., E. Roeckner, U. Mikolajewicz, and R. Voss (2000), Tropical stabilization of the thermohaline circulation in a greenhouse warming simulation, *Journal of Climate* 13, 1809-1813.
- Latif, M. (2001), Tropical Pacific/Atlantic ocean interactions at multi-decadal time scales, *Geophysical Research Letters* 28, 539-542.
- Lea, D. W., D. K. Pak, L. C. Peterson, and K. A. Hughen (2003), Synchronicity of tropical high latitude Atlantic temperatures over the last glacial termination, *Science* 301, 1361-1364.
- Magaña, V., J. A. Amador, and S. Medina (1999), The midsummer drought over Mexico and Central America, *Journal of Climate* 12, 1577-1588.
- Manabe, S., and R. J. Stouffer (1988), Two stable equilibria of a coupled ocean-atmosphere model, *Journal of Climate* 1, 841-866.
- Martínez, I., L. Keigwin, T. T. Barrows, Y. Yokoyama, and J. Southon (2003), La Niña-like conditions in the eastern equatorial Pacific and a stronger Choco jet in the northern Andes during the last glaciation, *Paleoceanography* 18, 10.1029/2002PA000877.
- McManus, J. F., D. W. Oppo, and J. L. Cullen (1999), A 0.5-million year record of millennial-scale climate variability in the North Atlantic, *Science* 283, 971-975.
- McManus, J. F., R. Francois, J. -M. Gherardi, L. D. Keigwin, and S. Brown-Leger (2004), Collapse and rapid resumption of Atlantic meridional circulation linked to deglacial climate changes, *Nature* 428, 834-837.
- Mix, A.C. (1985), *Paleoceanography and Paleoclimatology of the Tropical Atlantic: Evidence for Foraminifera and Stable Isotopes*, Ph.D. Dissertation, Columbia University, New York, 750 pp.

- National Oceanographic Data Center's Ocean Climate Laboratory (1998), *World Ocean Atlas 1998*, U.S. Gov. Printing Office, Washington, D.C.
- Oort, A. H. (1983), Global atmospheric circulation statistics, 1958-1973, *NOAA Prof. Pap. 14*, 180 pp.
- Oppo, D. W., J. F. McManus, and J. L. Cullen (2003), Deep water variability in the Holocene epoch, *Nature* 422, 277-278.
- Peterson, L. C., G. H. Haug, K. A. Hughen, and U. Röhl (2000), Rapid changes in the hydrologic cycle of the tropical Atlantic during the last glacial, *Science* 290, 1947-1951.
- Poveda, G., and O. J. Mesa (2000), On the existence of Lloró (the rainiest locality on Earth): Enhanced ocean-land-atmosphere interaction by a low-level jet, *Geophysical Research Letters* 27, 1675-1678.
- Rahmstorf, S. (1995), Bifurcations of the Atlantic thermohaline circulation in response to changes in the hydrological cycle, *Nature* 378, 145-149.
- Rodríguez-Rubio, E., W. Schneider, and R. Abarca del Río (2003), On the seasonal circulation within the Panama Bight derived from satellite observations of wind, altimetry and sea surface temperature, *Geophysical Research Letters* 30, doi:10.1029/2002GL016794.
- Schmidt, M. W., H. J. Spero, and D. W. Lea (2004), Links between salinity variation in the Caribbean and North Atlantic thermohaline circulation, *Nature* 428, 160-163.
- Schmittner, A., C. Appenzeller, and T. F. Stocker (2000), Enhanced Atlantic freshwater export during El Niño, *Geophysical Research Letters* 27, 1163-1166.
- Schmittner, A., and A. C. Clement (2002), Sensitivity of the thermohaline circulation to tropical and high latitude freshwater forcing during the last glacial-interglacial cycle, *Paleoceanography* 17, 10.1029/2000PA000591.
- Schulz, M., and K. Statterger (1997), Spectrum: Spectral analysis of unevenly spaced paleoclimatic time series, *Computers and Geosciences* 23, 929-945.
- Schulz, M., and M. Mudelsee (2002), REDFIT: Estimating red-noise spectra directly from unevenly spaced paleoclimatic time series, *Computers and Geosciences* 28, 421-426.

- Shackleton, N. J., M. A. Hall, and E. Vincent (2000), Phase relationships between millennial scale events 64,000 to 24,000 years ago, *Paleoceanography* 15, 565-569.
- Spero, H. J., K. M. Mielke, E. M. Kalve, D. W. Lea, and D. K. Pak (2003), Multispecies approach to reconstructing eastern equatorial Pacific thermocline hydrography during the past 360 ky, *Paleoceanography* 18, 10.1029/2002PA000814.
- Stott, L., C. Poulsen, S. Lund, and R. Thunell (2002), Super ENSO and global climate oscillations at millennial time scales, *Science* 297, 222-226.
- Stuiver, M., and P.J. Reimer (1993), Extended ^{14}C database and revised CALIB radiocarbon calibration program, *Radiocarbon* 35, 215-230.
- Takahashi, K., and D. S. Battisti (Submitted), Processes controlling the mean tropical Pacific precipitation pattern: I. The Andes and the eastern Pacific ITCZ, *Journal of Climate*.
- Thunell, R., E. Tappa, C. Pride, and E. Kincaid (1999), Sea-surface temperature anomalies associated with the 1997-1998 El Niño recorded in the oxygen isotope composition of planktonic foraminifera. *Geology* 27, 843-846.
- Vellinga, M., and R. A. Wood (2002), Global climatic impacts of a collapse of the Atlantic thermohaline circulation, *Climatic Change* 54, 251-267.
- Vellinga, M., and P. Wu (2004), Low-latitude freshwater influence on centennial variability of the Atlantic thermohaline circulation, *Journal of Climate* 17, 4498-4511.
- Waelbroeck, C., L. Labeyrie, E. Michel, J. C. Duplessy, J. F. McManus, K. Lambeck, E. Balbon, and M. Labracherie (2002), Sea-level and deep water temperature changes derived from benthic foraminifera isotopic records, *Quaternary Science Reviews* 21, 295-305.
- Weyl, P. K. (1968), The role of the oceans in climatic change: A theory of the ice ages, *Meteorological Monographs* 8, 37-62.
- Xie, S., H. Xu, W. S. Kessler, and M. Nonaka (2005), Air-sea interaction over the eastern Pacific warm pool: Gap winds thermocline dome, and atmospheric convection, *Journal of Climate* 18, 5-20.
- Xu, H., S. Xie, Y. Wang, and R. J. Small (2005), Effects of Central American mountains on the eastern Pacific winter ITCZ and moisture transport, *Journal of Climate* 18, 3856-3873.
- Zaucker, F., T. F. Stocker, and W. S. Broecker (1994), Atmospheric freshwater fluxes

and their effect on the global thermohaline circulation, *Journal of Geophysical Research* 99, 12,443-12,457.

Zhang, R. and T. L. Delworth (2005), Simulated tropical response to a substantial weakening of the Atlantic thermohaline circulation, *Journal of Climate* 18, 1853-1860.

Zheng, Y., A. van Geen, R. F. Anderson, J. V. Gardner, and W. E. Dean (2000), Intensification of the northeast Pacific oxygen minimum zone during the Bølling-Allerød warm period, *Paleoceanography* 15, 528-536.

Acknowledgments. W. Rugh, M. Cheseby, J. Padman, M. Phipps, A. Ross, and A. Ungerer provided laboratory assistance. J. Chaytor and C. Chickadel provided assistance with Figure 1. Reviews from E. Maloney and A. Schmittner greatly improved the manuscript. The authors thank shipboard participants of NEMO-3 (2000) and the Ocean Drilling Program Leg 202 for helpful discussion and assistance with sampling. N. Pisias provided assistance with statistical analyses. Comments from two anonymous reviewers greatly improved the manuscript. Support for this research was provided by the U.S. National Science Foundation.

Auxiliary Material

Data tables 1-4: Table 1 = age model information; Table 2 = core top data; Table 3 = ME0005A-43JC downcore data; Table 4 = ODP 1242 downcore data

Figure Captions

Figure 1. Annual average salinity (PSU) for the Eastern Pacific Warm Pool (EPWP) region and the western Caribbean [*World Ocean Atlas*, 1998]. Pacific sites (ME0005A-43JC: 7° 51.35'N, 83° 36.50'W, 1368 m and ODP Site 1242: 7° 51.35'N, 83° 36.42'W, 1364 m) used in this study are indicated. **Inset:** T-S diagram [*World Ocean Atlas*, 1998] of the EPWP region with isopycnals (red dotted) and predicted $\delta^{18}\text{O}_c$ isolines (black solid) calculated from temperature and salinity [*Bemis et al.*, 1998] assuming modern regional $\delta^{18}\text{O}_{\text{sw-S}}$ [*Benway and Mix*, 2004].

Figure 2. A north-south transect of sites in the eastern tropical Pacific with corresponding profiles of **A.** Predicted $\delta^{18}\text{O}_c$ at 0, 50, and 100 m, which is calculated from cultured *O. universa* high light (0 m) and low light (50, 100 m) equations [Bemis *et al.*, 1998]. Red (blue) symbols indicate measured $\delta^{18}\text{O}_c$ of *G. ruber* (*N. dutertrei*) in multi-core tops at each site. **B.** Annual average temperature at 0, 50, and 100 m [World Ocean Atlas, 1998]. Red symbols indicate Mg/Ca-based temperature estimates from *G. ruber* in multi-core tops at each site. Mg/Ca is converted to temperature using the calibration equation of Anand *et al.* [2003]. Core top Mg/Ca and $\delta^{18}\text{O}_c$ measurements verify that the depth habitat of *G. ruber* is in the upper mixed layer. The $\delta^{18}\text{O}_c$ multi-core data for *N. dutertrei* verify that the depth habitat of this species is near the base of the thermocline, which is ~50-75 m at these coring sites (ME0005A-43JC, ODP 1242).

Figure 3. Data from ME0005A-43JC (filled symbols) and ODP Site 1242 (unfilled symbols). Ages reported in calendar ky before present. AMS ^{14}C dates for ME0005A-43JC are indicated by filled circles on age axis with 2-sigma error bars. **A.** $\delta^{18}\text{O}_c$ for *G. ruber* (white) and *N. dutertrei*. **B.** $\delta^{18}\text{O}_c$ difference between *G. ruber* and *N. dutertrei*, indicating upper ocean contrast above the pycnocline. **C.** Mg/Ca-based temperature for *G. ruber*. Mg/Ca was converted to temperature using $\text{Mg/Ca} = 0.38\text{Exp}(0.090T)$ [Anand *et al.*, 2003]. Modern annual average surface temperature [World Ocean Atlas, 1998] is indicated on the y-axis. **D.** $\delta^{18}\text{O}_{\text{sw}}$ estimates calculated from *G. ruber* Mg/Ca and $\delta^{18}\text{O}_c$ [Bemis *et al.*, 1998; Thunell *et al.*, 1999] and corrected for ice volume changes [Clark and Mix, 2002; Waelbroeck *et al.*, 2002]. The potential range of $\delta^{18}\text{O}_{\text{sw}}$ uncertainty

associated with ice volume change is indicated by the two red curves. The bold curve indicates a scaling of 0.01‰ m^{-1} while the thin dashed curve indicates a scaling of 0.0075‰ m^{-1} decrease in relative sea level (RSL). The resulting range of uncertainty in the corrected $\delta^{18}\text{O}_{\text{sw}}$ is indicated by the corresponding bold and thin dashed black smoothed $\delta^{18}\text{O}_{\text{sw}}$ records. The modern measured $\delta^{18}\text{O}_{\text{sw}}$ [*World Ocean Atlas*, 1998] is indicated on the y-axis. For the combined records of the two sites a Gaussian smoothing function (time step = 0.2 ky; filter width = 0.8 ky) was applied.

Figure 4 A. Sea-surface temperature (SST) reconstructions from Cariaco Basin core PL07-39PC [*Lea et al.*, 2003] based on Mg/Ca (red) and subtropical northeast Atlantic core SU8118 [*Bard*, 2002] based on alkenones (black). **B.** Measured color reflectance (550 nm) [*Peterson et al.*, 2000] and % Ti [*Haug et al.*, 2001] of Cariaco Basin sediments, ODP Site 1002. Lower reflectance (darker, clay-rich sediment) and higher % Ti (increased terrigenous sediment) imply wetter conditions in northern South America. **C.** $\delta^{18}\text{O}_{\text{sw}}$ and estimated paleosalinity from the EPWP (ME0005A-43JC and ODP Site 1242) [*Benway and Mix*, 2004] and the Caribbean [*Schmidt et al.*, 2004]. The same ice volume correction is applied to both records (see bold red curve, Fig. 3d), and two separate salinity scales are shown, based on regional $\delta^{18}\text{O-S}$ [*Benway and Mix*, 2004; *Schmidt et al.*, 2004]. Black circles indicate Caribbean radiocarbon age control points with 2-sigma error bars. Pacific radiocarbon age control points are shown in Fig. 3D. **D.** Estimates of interbasin salinity average based on averaging Pacific and Caribbean [*Schmidt et al.*, 2004] $\delta^{18}\text{O}_{\text{sw}}$. Upward arrow indicates southward ITCZ position. The

higher resolution Pacific record was first placed on the Caribbean time scale using Gaussian interpolation, the records were differenced, and the result was smoothed (0.2 ky time step, filter width = 0.8 ky). Gray curves show maximum age model error in the interbasin contrast calculation, based on 2-sigma ranges in Pacific and Caribbean radiocarbon dates. **E.** Estimates of interbasin salinity contrast based on differencing Pacific and Caribbean [*Schmidt et al.*, 2004] $\delta^{18}\text{O}_{\text{sw}}$. Upward arrow indicates increased water vapor transport. See above (4D) for details on calculations. **F.** $^{231}\text{Pa}/^{230}\text{Th}$ ratios (calculated from measured ^{238}U activity) from Bermuda rise [*McManus et al.*, 2004], indicating strength of Atlantic meridional overturning circulation (MOC). Black circles indicate Bermuda Rise radiocarbon age control points with 2-sigma error bars. Benthic $\delta^{13}\text{C}$ records from MD95-2042 [*Shackleton et al.*, 2000], V30-51K [*Mix*, 1985], and ODP Site 980 [*McManus et al.*, 1999; *Oppo et al.*, 2003] also indicate changes in deep ocean circulation. **G.** GISP2 $\delta^{18}\text{O}_{\text{ice}}$ [*Grootes and Stuiver*, 1997], indicating high latitude air temperatures. Cold (blue shaded bars) and warm (or sealevel rise) events (red shaded bars) of the last 30 ky are indicated. 8 ka = 8.2 ka event; YD = Younger Dryas; HE-1, 2, 3 = Heinrich events; 19 ka = earliest postglacial sealevel rise; T-1A = Termination or meltwater pulse (MWP)-1A; T-1B = Termination or MWP-1B.

Figure 5. Spectral calculations based on a Schultz fast fourier transform that allows for non-constant delta-T [*Schulz and Stattegger*, 1997; *Schulz and Mudelsee*, 2002] for the **A.** Holocene (0-10 ka) and **B.** Glacial and deglacial (10-30 ka) portions of the EPWP

$\delta^{18}\text{O}_{\text{sw}}$ record. Bandwidths and degrees of freedom are indicated. The dotted-dashed lines represent the 95% confidence intervals.

Figure 6. Cross-spectral, coherency, and phase calculations based on a Schultz fast fourier transform that allows for non-constant delta-T [Schulz and Stattegger, 1997; Schulz and Mudelsee, 2002] comparing EPWP $\delta^{18}\text{O}_{\text{sw}}$ (solid) with Caribbean $\delta^{18}\text{O}_{\text{sw}}$ (dashed) [Schmidt et al., 2004]. Phases are only calculated for Coh^2 values that exceed the 90% confidence level. Positive (negative) phases indicate a lead (lag) of the EPWP $\delta^{18}\text{O}_{\text{sw}}$ relative to Caribbean $\delta^{18}\text{O}_{\text{sw}}$. Bandwidths and 90% confidence levels are indicated.

Figure 7. Cross-spectral, coherency, and phase calculations based on a Schultz fast fourier transform that allows for non-constant delta-T [Schulz and Stattegger, 1997; Schulz and Mudelsee, 2002] comparing **A.** Interbasin salinity contrast (solid) with Atlantic MOC (dashed) [McManus et al., 2004], and **B.** EPWP $\delta^{18}\text{O}_{\text{sw}}$ (solid) with Atlantic MOC (dashed) [McManus et al., 2004]. Phases are only calculated for Coh^2 values that exceed the 90% confidence level. Positive (negative) phases indicate a lead (lag) of the interbasin contrast and EPWP records relative to Atlantic MOC. Bandwidths and 90% confidence levels are indicated.

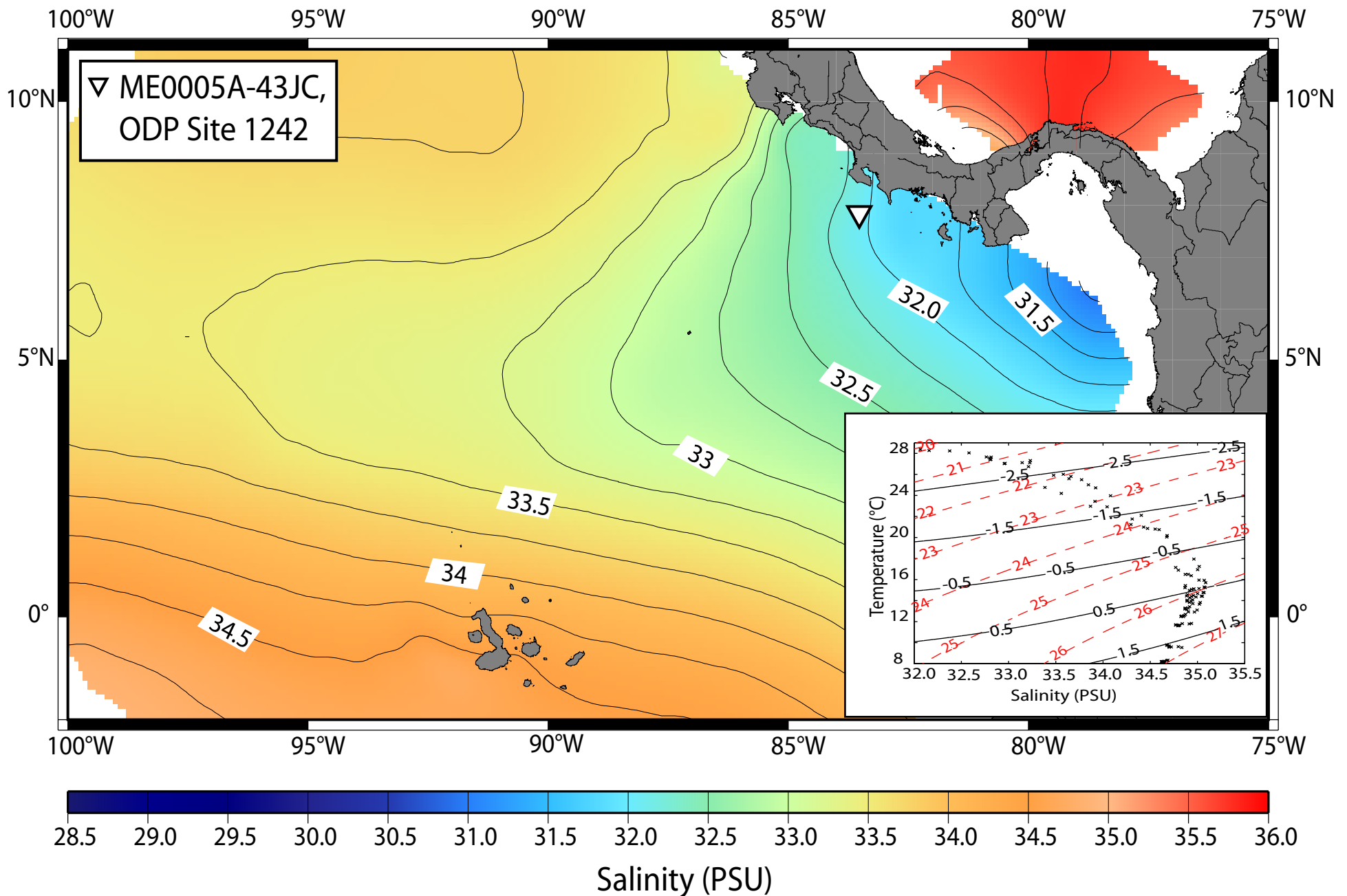


Figure 1. Annual average salinity (PSU) for the Eastern Pacific Warm Pool (EPWP) region and the western Caribbean [World Ocean Atlas, 1998]. Pacific sites (ME0005A-43JC: 7° 51.35'N, 83° 36.50'W, 1368 m and ODP Site 1242: 7° 51.35'N, 83° 36.42'W, 1364 m) used in this study are indicated. Inset: T-S diagram [World Ocean Atlas, 1998] of the EPWP region with isopycnals (red dotted) and predicted $\delta^{18}\text{O}_c$ isolines (black solid) calculated from temperature and salinity [Bemis et al., 1998] assuming modern regional $\delta^{18}\text{O}_{\text{sw-S}}$ [Benway and Mix, 2004].

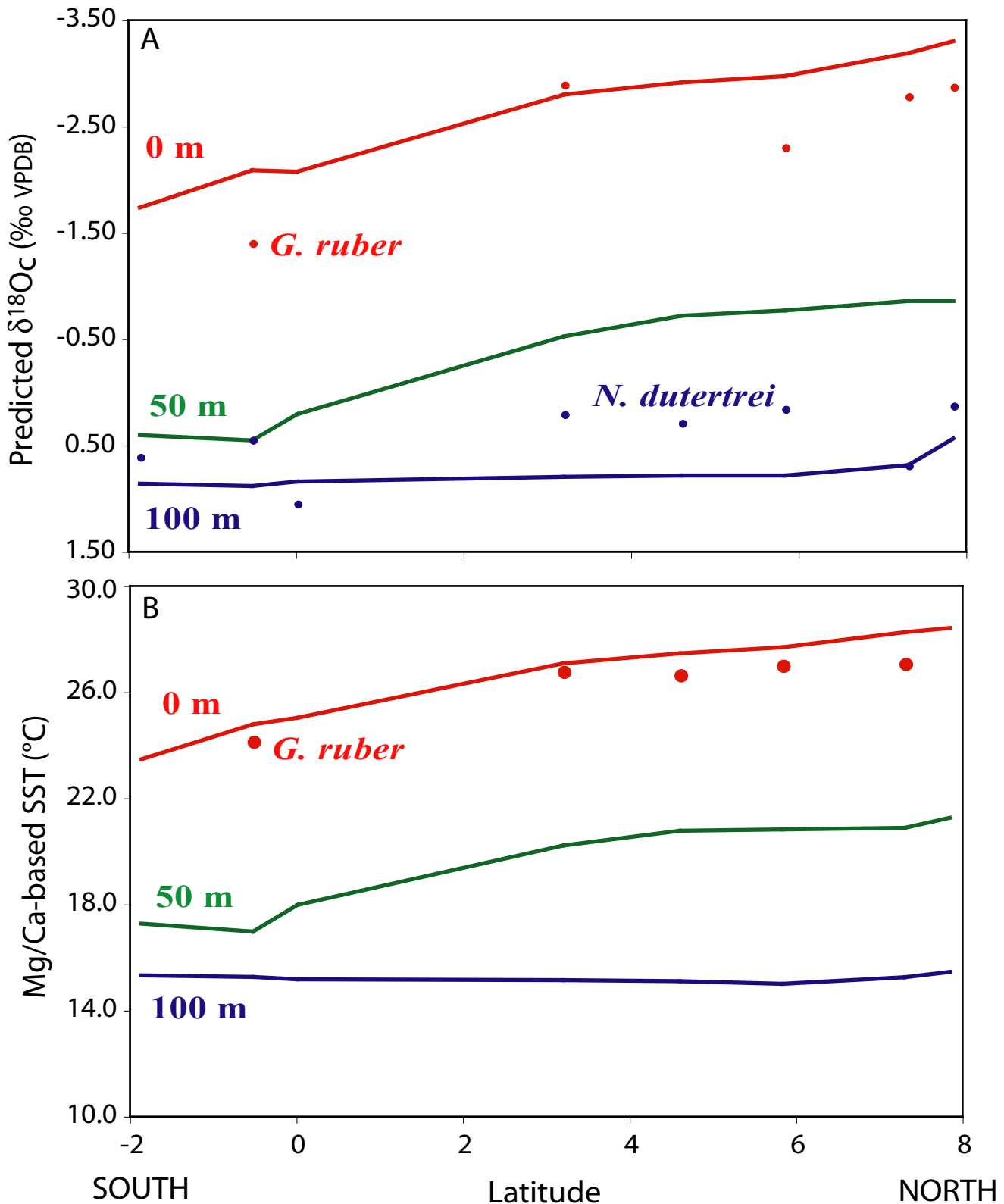


Figure 2. A north-south transect of sites in the eastern tropical Pacific with corresponding profiles of **A.** Predicted $\delta^{18}\text{O}_c$ at 0, 50, and 100 m, which is calculated from cultured *O. universa* high light (0 m) and low light (50, 100 m) equations [Bemis *et al.*, 1998]. Red (blue) symbols indicate measured $\delta^{18}\text{O}_c$ of *G. ruber* (*N. dutertrei*) in multi-core tops at each site. **B.** Annual average temperature at 0, 50, and 100 m [World Ocean Atlas, 1998]. Red symbols indicate Mg/Ca-based temperature estimates from *G. ruber* in multi-core tops at each site. Mg/Ca is converted to temperature using the calibration equation of Anand *et al.* [2003]. Core top Mg/Ca and $\delta^{18}\text{O}_c$ measurements verify that the depth habitat of *G. ruber* is in the upper mixed layer. The $\delta^{18}\text{O}_c$ multi-core data for *N. dutertrei* verify that the depth habitat of this species is near the base of the thermocline, which is ~50-75 m at these coring sites (ME0005A-43JC, ODP 1242).

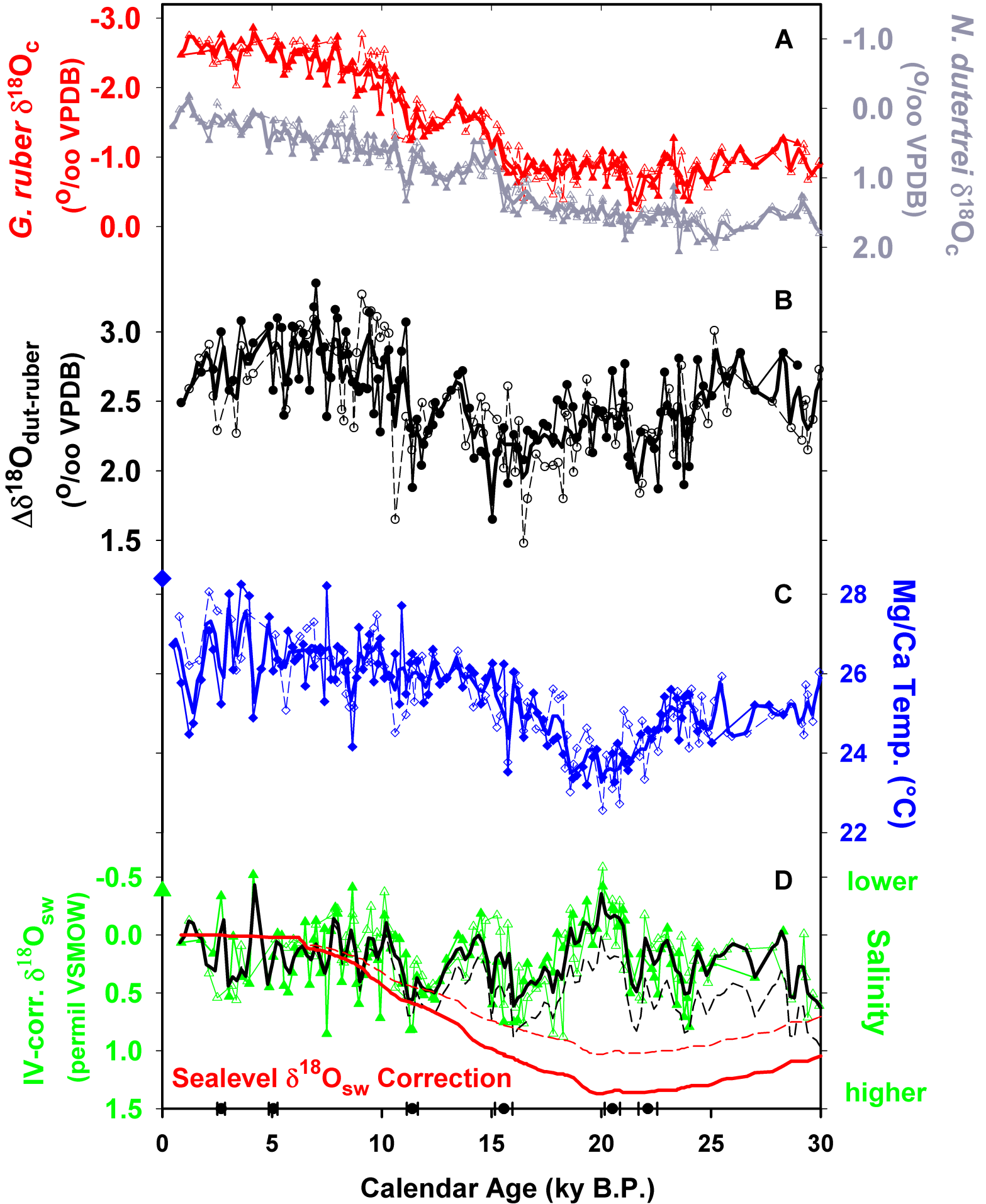


Figure 3

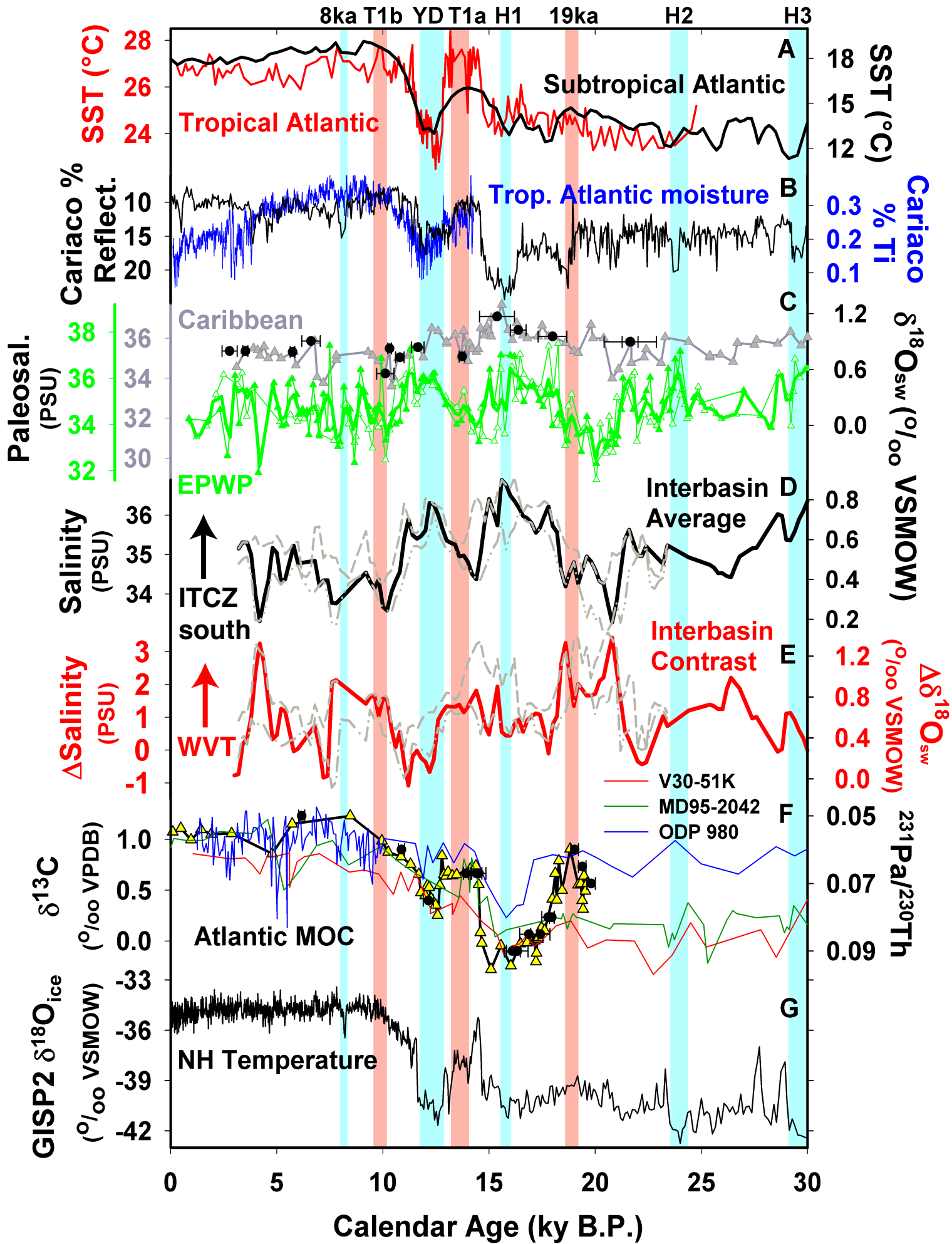
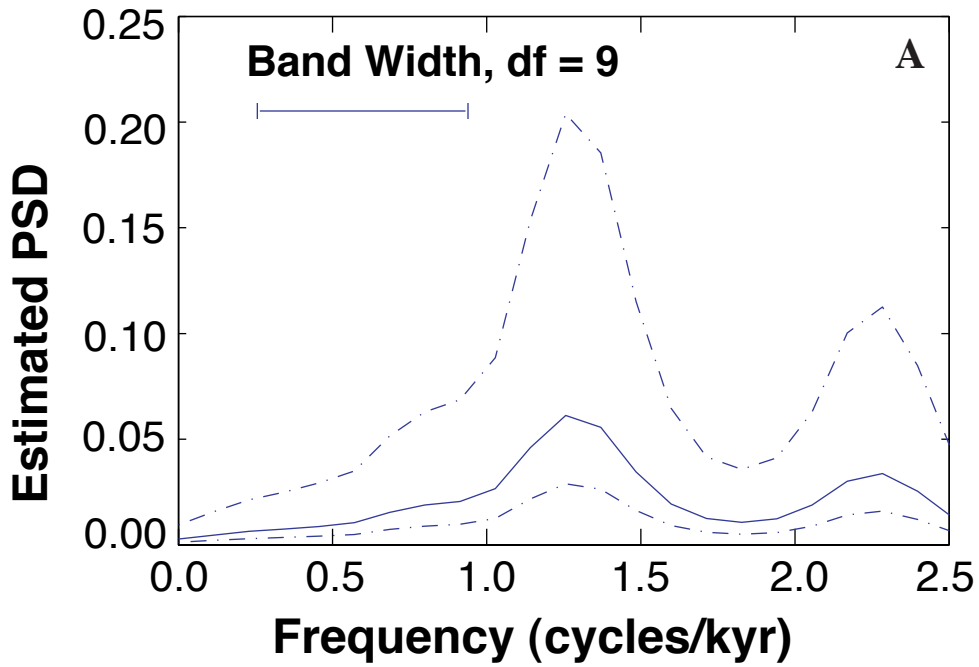


Figure 4

**Holocene (0-10 ka)
EPWP $\delta^{18}\text{O}_{\text{sw}}$**



**Glacial/Deglacial (10-30 ka)
EPWP $\delta^{18}\text{O}_{\text{sw}}$**

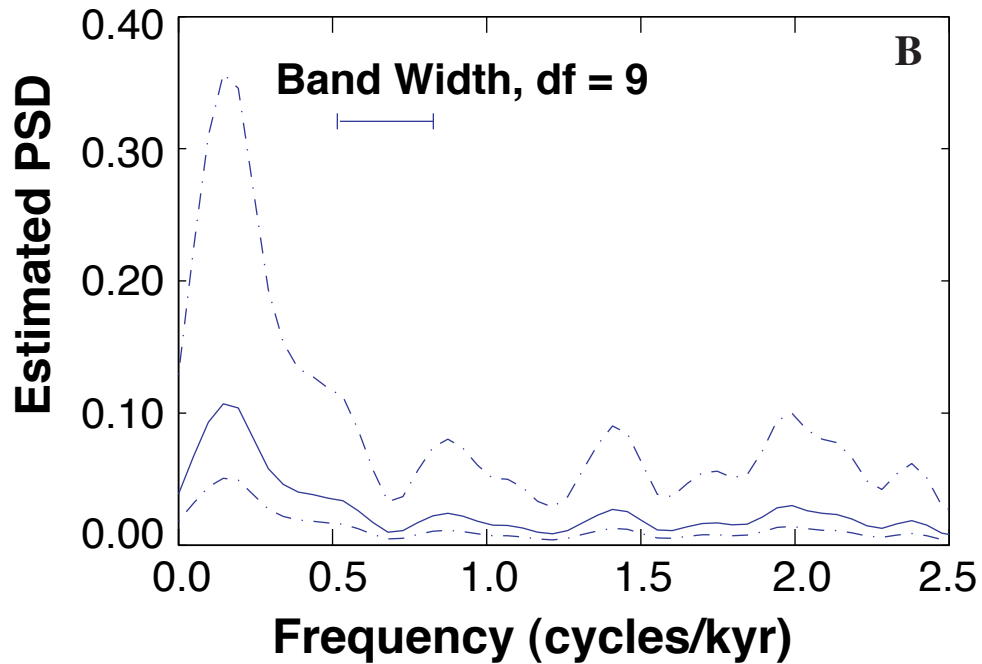


Figure 5

Pacific $\delta^{18}\text{O}_{\text{sw}}$ vs. Caribbean $\delta^{18}\text{O}_{\text{sw}}$

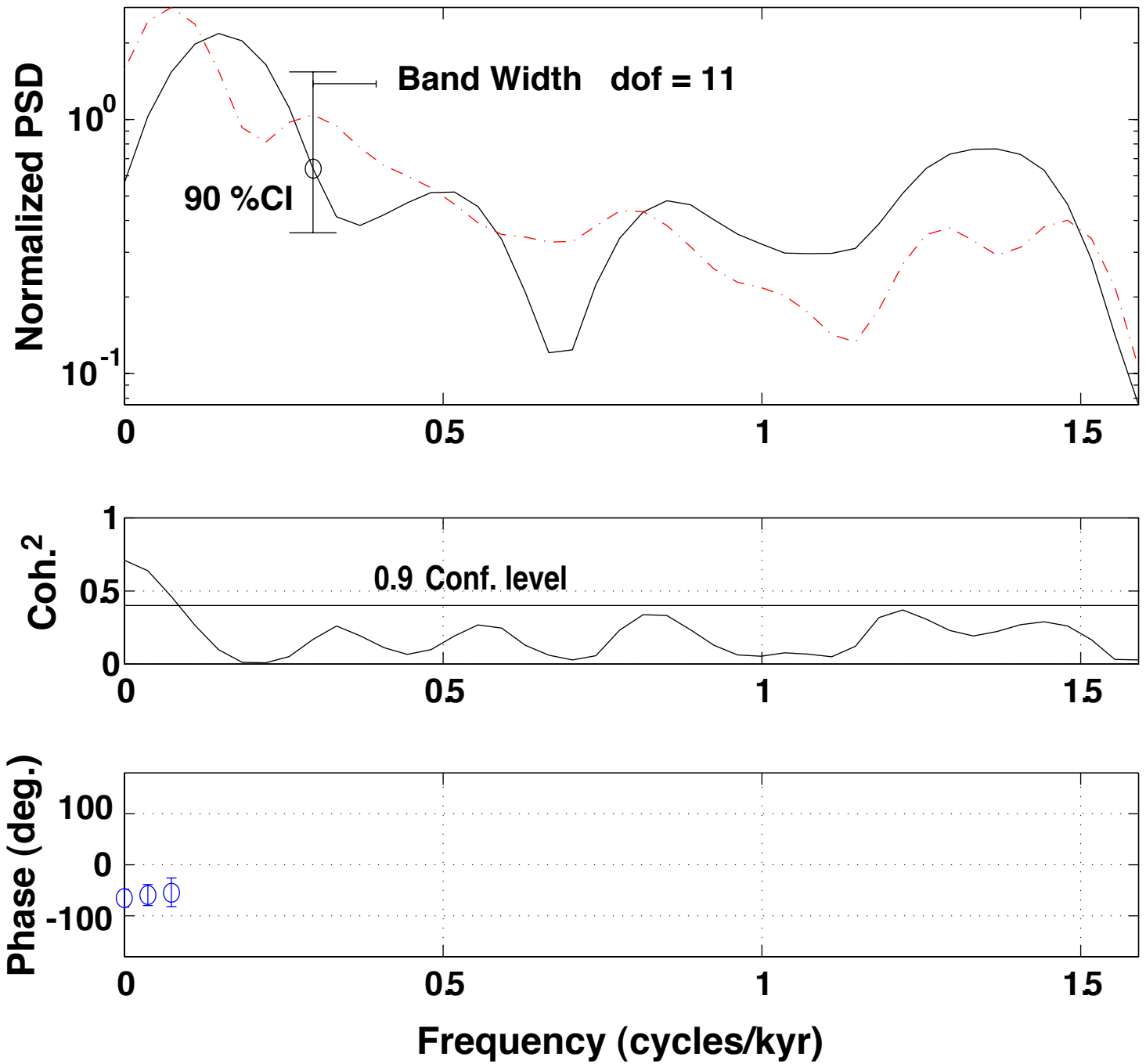
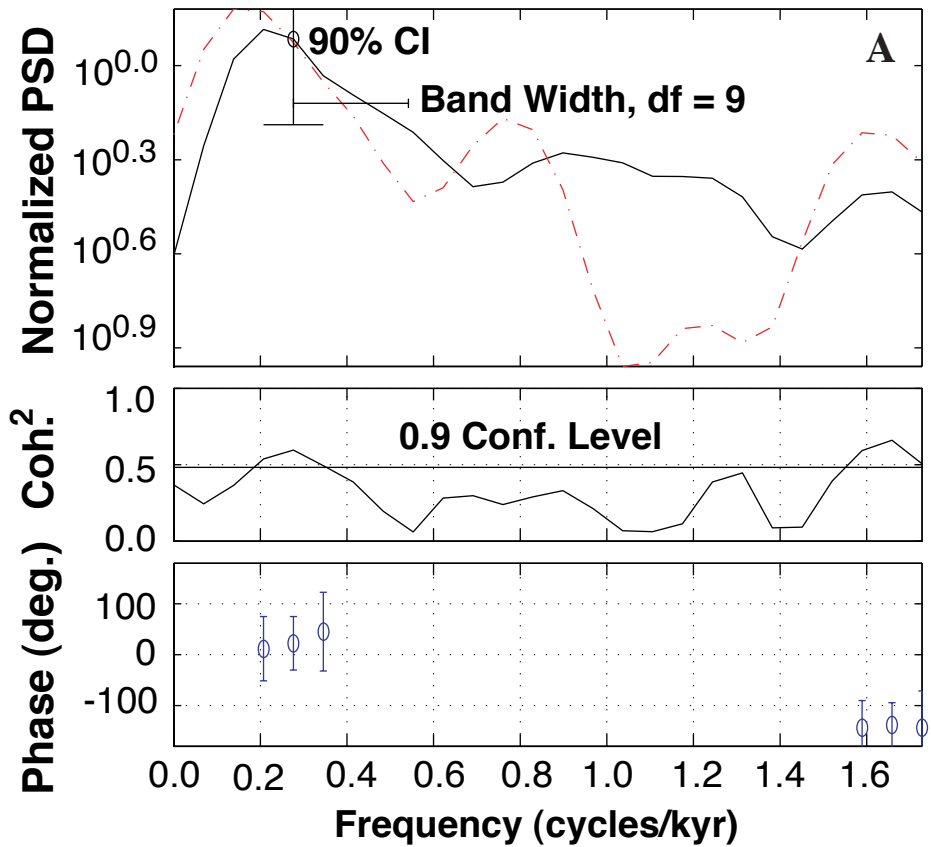


Figure 6

Interbasin salinity contrast vs. Atlantic MOC



Pacific $\delta^{18}\text{O}_{\text{sw}}$ vs. Atlantic MOC

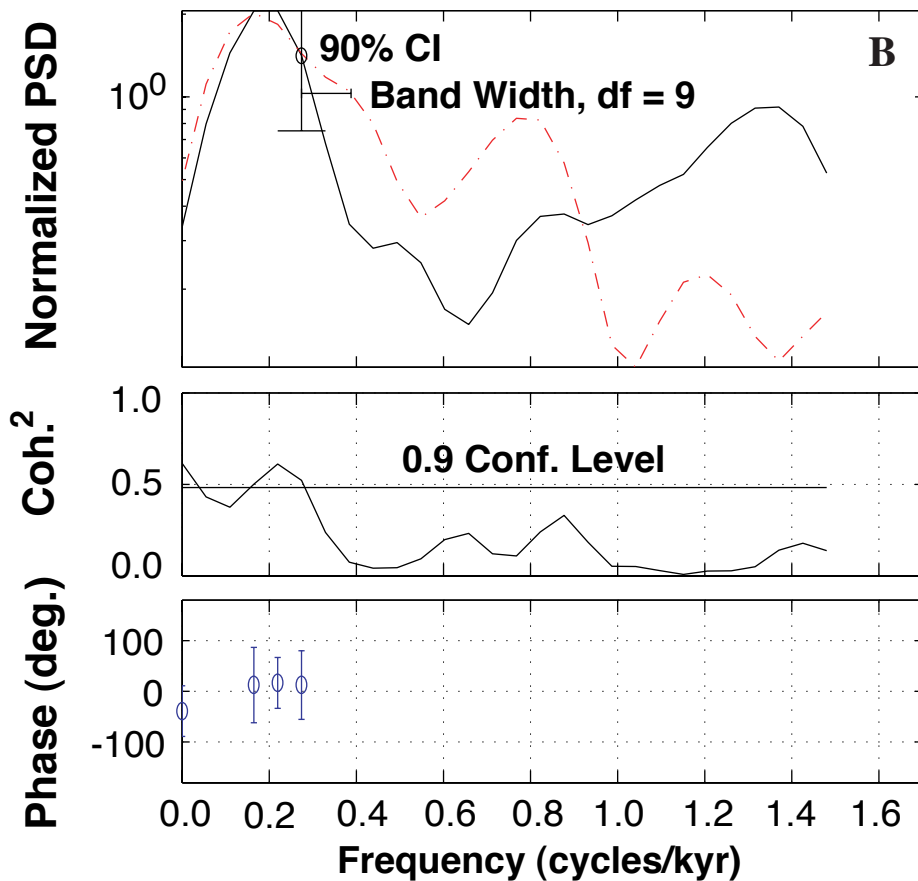


Figure 7